GSK1838705A inhibits the insulin-like growth factor-1 receptor and anaplastic lymphoma kinase and shows antitumor activity in experimental models of human cancers

Peter Sabbatini,[1] Susan Korenchuk,[1] Jason L. Rowand,[1] Arthur Groy,[1] Qi Liu,[1] Dominic Leperi,[1] Charity Atkins,[1] Melissa Dumble,[1] Jingsong Yang,[1] Kelly Anderson,[1] Ryan G. Kruger,[1] Richard R. Gontarek,[1] Kenneth R. Maksimchuk,[1] Sapna Suravajjala,[1] Russell R. Lapierre,[1] J. Brad Shotwell,[2] Joseph W. Wilson,[2] Stanley D. Chamberlain,[2] Sridhar K. Rabindran,[1] and Rakesh Kumar[1]

[1]Oncology R&D, GlaxoSmithKline, Collegeville, Pennsylvania and [2]GlaxoSmithKline, Research Triangle Park, North Carolina

Abstract

The insulin-like growth factor-I receptor (IGF-IR) signaling pathway is activated in various tumors, and inhibition of IGF-IR kinase provides a therapeutic opportunity in these patients. GSK1838705A is a small-molecule kinase inhibitor that inhibits IGF-IR and the insulin receptor with IC_{50}s of 2.0 and 1.6 nmol/L, respectively. GSK1838705A blocks the *in vitro* proliferation of cell lines derived from solid and hematologic malignancies, including multiple myeloma and Ewing's sarcoma, and retards the growth of human tumor xenografts *in vivo*. Despite the inhibitory effect of GSK1838705A on insulin receptor, minimal effects on glucose homeostasis were observed at efficacious doses. GSK1838705A also inhibits the anaplastic lymphoma kinase (ALK), which drives the aberrant growth of anaplastic large-cell lymphomas, some neuroblastomas, and a subset of non–small cell lung cancers. GSK1838705A inhibits ALK, with an IC_{50} of 0.5 nmol/L, and causes complete regression of ALK-dependent tumors *in vivo* at well-tolerated doses. GSK1838705A is therefore a promising antitumor agent for therapeutic use in human cancers. [Mol Cancer Ther 2009;8(10):2811–20]

Received 5/13/09; revised 8/5/09; accepted 8/6/09; published 10/12/09.

The costs of publication of this article were defrayed in part by the payment of page charges. This article must therefore be hereby marked *advertisement* in accordance with 18 U.S.C. Section 1734 solely to indicate this fact.

Note: Supplementary material for this article is available at Molecular Cancer Therapeutics Online (http://mct.aacrjournals.org/).

Requests for reprints: Rakesh Kumar, Oncology R&D, Cancer Research, GlaxoSmithKline, 1250 South Collegeville Road, Collegeville, PA 19426. Phone: 610-917-4855; Fax: 610-917-4181. E-mail: rakesh.2.kumar@gsk.com

doi:10.1158/1535-7163.MCT-09-0423

Introduction

The insulin-like growth factor-I receptor (IGF-IR) signaling pathway is dysregulated in many human cancers, including prostate, colon, breast, pancreatic, liver, and ovarian cancers and sarcomas, due to aberrant expression of IGF-IR or its ligands, IGF-I and IGF-II (1–4). Decreased levels of IGF binding proteins (IGFBP), which bind and sequester the ligands and prevent them from activating the receptor, also contribute to the activation of this pathway (2–4). IGF-IR is required for transformation of mouse embryonic fibroblasts by a variety of oncogenes, including SV40 T antigen, the human papillomavirus E5 and E7 proteins, Ewing's sarcoma fusion protein, Ha-ras, c-src, epidermal growth factor receptor, and platelet-derived growth factor receptor (5). Furthermore, inhibition of IGF-IR signaling using antibodies, antisense, IGFBPs, small interfering RNA, and dominant-negative receptor results in decreased proliferation and survival of tumor cells *in vitro* and *in vivo* (6–8). More recently, monotherapy with anti–IGF-IR antibodies has shown clinical activity in patients with multiple myeloma and sarcoma (9, 10). A study combining IGF-IR antibodies with paclitaxel and carboplatin in non–small cell lung cancer (NSCLC) patients showed an improved response rate compared with chemotherapy alone (11). Resistance to targeted agents, such as inhibitors of epidermal growth factor receptor and ErbB2, has been associated with IGF-IR activation, suggesting that inhibition of IGF-IR signaling may reverse resistance to these agents (12–14).

We describe here the biochemical, cellular, and pharmacologic characteristics of the 1*H*-pyrrolo[2,3-*d*]pyrimidine, GSK1838705A, a novel inhibitor of IGF-IR and insulin receptor (IR) activity. Because this compound is also a potent inhibitor of anaplastic lymphoma kinase (ALK), the antitumor activity in ALK-driven tumors is shown.

Materials and Methods

Compounds

GSK1838705A was synthesized at GlaxoSmithKline (Table 1) and dissolved in DMSO at 10 mmol/L for *in vitro* studies. The compound was formulated in 20% sulfobutyl ether β-cyclodextrin (ISP; pH 3.5) for *in vivo* studies.

Kinase Assays

Baculovirus-expressed glutathione *S*-transferase–tagged proteins encoding the intracellular domain of IGF-IR (amino acids 957–1367) and IR (amino acids 979–1382) were used for determinations of IC_{50}s by a homogeneous time-resolved fluorescence assay. A filter binding assay was used for $^{app}K_i$ determinations using activated IGF-IR and IR kinases (details of the assays are available in Supplementary Data). Expanded kinase-selectivity profiling of GSK1838705A was

Table 1. Activity of GSK1838705A in kinase-selectivity panel

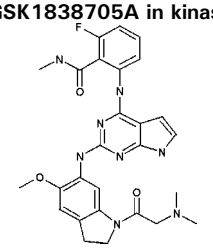

Kinase	IC_{50} (nmol/L)	Kinase	IC_{50} (nmol/L)
AKT1	>10,000	JNK1	5,000
AKT2	>10,000	JNK2	8,000
ALK	0.5	JNK3	2,000
ALK5	>10,000	LCK	>25,000
ASK1	>25,000	MAPKAPK2	>25,000
Aurora A	>10,000	P38a	>25,000
Aurora B	>10,000	PAK1	>10,000
B-Raf V600E	>2,000	PCTAIRE1	>10,000
CAMKK2	>10,000	PDK1	>10,000
CDK2/CyclinA	>10,000	PI3Kα	>10,000
EGFR	>10,000	PI3Kβ	>10,000
ErbB2	>10,000	PI3Kδ	>10,000
ErbB4	>25,000	PI3Kγ	>10,000
GSK3β	>25,000	PKCε	>10,000
HGK	>10,000	PKCq	>10,000
IGF-IR	1.6	ROCK1	>10,000
IKK1	>25,000	RSK1	1,600
IKK2	>25,000	SRC1	>10,000
IKK3	>10,000	SYK	>25,000
ITK	>25,000	VEGFR2	>10,000
IR	2	YAK3	>10,000
JAK1	>25,000	ZAP70	>25,000
JAK2	13,000	P70S6K	>10,000
JAK3	5,000		

carried out by screening the compound in the KinaseProfiler panel (Millipore).

Animals

Eight- to 12-week-old female nu/nu CD-1 mice (Charles River Laboratories) and severe combined immunodeficient (SCID) mice (Taconic Farms) were handled in compliance with the Institutional Animal Care and Use Committee guidelines.

Cell Lines and Culture

Cell lines were purchased from either the American Type Culture Collection or the German Collection of Microorganisms and Cell Cultures (DSMZ). NIH-3T3 cells that overexpress human IGF-IR (NIH-3T3/LISN) or IR (NIH-3T3-hIR) were obtained from Dr. Michael Kaleko (Fred Hutchinson Cancer Research Center, Seattle, WA; ref. 15). Anaplastic large-cell lymphoma (ALCL) FE-PD cells were provided by Dr. Annarosa Del Mistro (Istituto Oncologico Veneto, IRCCS, Padova, Italy).

Receptor Phosphorylation Assays

NIH-3T3/LISN and NIH-3T3-hIR cell lines were seeded in culture medium in collagen-coated 96-well tissue culture plates (BD Biosciences). After 24 h, cells were treated with DMSO or various concentrations of GSK1838705A (diluted in DMSO, 0.2% final concentration in assay) and stimulated 2 h later with either 30 ng/mL human IGF-I or 3 μg/mL bovine insulin (Sigma Aldrich) for 15 min. Cells were lysed in radioimmunoprecipitation assay buffer [150 mmol/L NaCl, 50 mmol/L Tris-Cl (pH 7.5), 0.25% sodium deoxycholate, 1% NP40, protease inhibitors (Roche Diagnostics), and 100 mmol/L sodium orthovanadate (Sigma Aldrich)]. Lysates were transferred to 96-well assay plates (MaxiSorp, NalgeNunc) previously coated with either anti–IGF-IR (R&D Systems) or anti-IRβ (Santa Cruz Biotechnology) at 4°C overnight. Plates were washed and treated with Eu-labeled phosho-tyrosine antibody PT66 (Perkin-Elmer) for the detection of phosphorylated IGF-IR and IR. Total IGF-IR and IR were detected with anti–IGF-IRβ (Santa Cruz Biotechnology) or anti-IR (Lab Vision/Thermo Fisher Scientific), respectively. Secondary antibodies used were Eu-labeled goat anti-rabbit IgG (for IGF-IR) and Eu-labeled goat anti-mouse IgG (for IR; Perkin-Elmer). Eu fluorescence was quantified using a Victor Multilabel Counter (Perkin-Elmer; excitation 340 nm/emission 615 nm). EC_{50} values were determined from concentration-response curves using XLfit4 software (Guildford).

Phosphorylation assays for phospho-ALK (Tyr-1604) were carried out using commercial assays (Cell Signaling Technologies).

Cell Proliferation Assays

Cells were seeded in 96-well dishes, incubated overnight at 37°C, and treated with DMSO or GSK1838705A for 72 h. For the NIH-3T3/LISN proliferation assays, cells were seeded on collagen-coated 96-well tissue culture plates (BD Biosciences) and allowed to adhere for 24 h. The medium was replaced with serum-free medium and the cells were treated with GSK1838705A for 2 h. Cells were incubated for 72 h after addition of IGF-I (30 ng/mL). Cell proliferation was quantified using the CellTiter-Glo Luminescent Cell Viability Assay (Promega). IC_{50}s were determined from cytotoxicity curves using a four-parameter curve fit software package (XLfit4).

Western Blotting

Cells were treated with DMSO or GSK1838705A, washed, and lysed in cold radioimmunoprecipitation assay buffer. Clarified lysates were resolved by SDS-PAGE (Invitrogen) and proteins were transferred to nitrocellulose. Blots were incubated with antibodies to phospho-IGF-IR/IR (Tyr-1135/1136), extracellular signal–regulated kinase (ERK), phospho-ERK (Thr-202/Tyr204), AKT, phospho-AKT (Ser-473), ALK, phospho-ALK (Tyr-1604), STAT3, phospho-STAT3 (Tyr-705; Cell Signaling Technologies); IRS-1, phospho-IRS-1 (Tyr-989), and IGF-IR (Santa Cruz Biotechnology). Antibodies to actin (Sigma Aldrich) were used to show equal sample loading. Secondary antibodies used were IRDye 700DX–labeled goat anti-mouse IgG and IRDye 800-CW goat anti-rabbit IgG (Rockland Immunochemicals). Proteins were detected on the Odyssey Infrared Imager (Li-Cor Biosciences).

Flow Cytometry

Exponentially growing cells were seeded into 96-well tissue culture plates overnight at 37°C and treated with GSK1838705A for 24 and 48 h. Plates were processed for

flow cytometry using the Vindelov method (16). Cell cycle analyses were done using a FACSCalibur (BD Biosciences) and FlowJo software (Tree Star, Inc.).

In vivo Efficacy Studies

Exponentially growing cells were implanted s.c. into the right flank of 8- to 12-wk-old female nu/nu CD-1 or SCID mice. When the tumors reached ~200 mm^3 in size, the animals were weighed and block randomized according to tumor size into treatment groups of eight mice each. Mice were dosed p.o. with the formulating vehicle or GSK1838705A. Mice were weighed and tumors measured by calipers twice weekly. Tumor volumes were calculated using the following formula: tumor volume = (length × $width^2$)/2. The percentage of tumor growth inhibition was calculated on each day of tumor measurement using the following formula: 100 × [1 − (average growth of the compound-treated tumors/average growth of vehicle-treated control tumors)].

Metabolic Studies

Blood glucose and β-hydroxybutyrate levels were measured using commercially available devices [Accucheck (Roche Diagnostics) and MediSense Precision Xtra (Abbott), respectively]. Plasma insulin levels were measured by ELISA (Crystal Chem).

Pharmacodynamic Studies

For IGF-IR pharmacodynamic studies, female nu/nu CD-1 mice bearing NIH-3T3/LISN or COLO 205 tumors ~500 mm^3 in size were given a single oral dose of vehicle or GSK1838705A. Four hours later, 10 μg of hIGF-I (via the tail vein) were administered, and animals were euthanized after 10 min for collection of tumor tissue and blood. Frozen tumors samples were homogenized in radioimmunoprecipitation assay buffer and tumor lysates were transferred to chilled IGF-IR capture plates. The plates were then processed for the quantification of phosphorylated IGF-IR and total IGF-IR as described for the cell-based phosphorylation assays. For signal transduction studies, tumor cell lysates were analyzed by Western blotting. ALK pharmacodynamic studies were done in SCID mice bearing Karpas-299 tumors. The studies were done similar to the outline above, but without the addition of IGF-I. Tumor cell lysates were analyzed by Western blotting. Antibodies to full-length and cleaved caspase-3, caspase-7, and poly(ADP-ribose) polymerase were obtained from Cell Signaling Technologies.

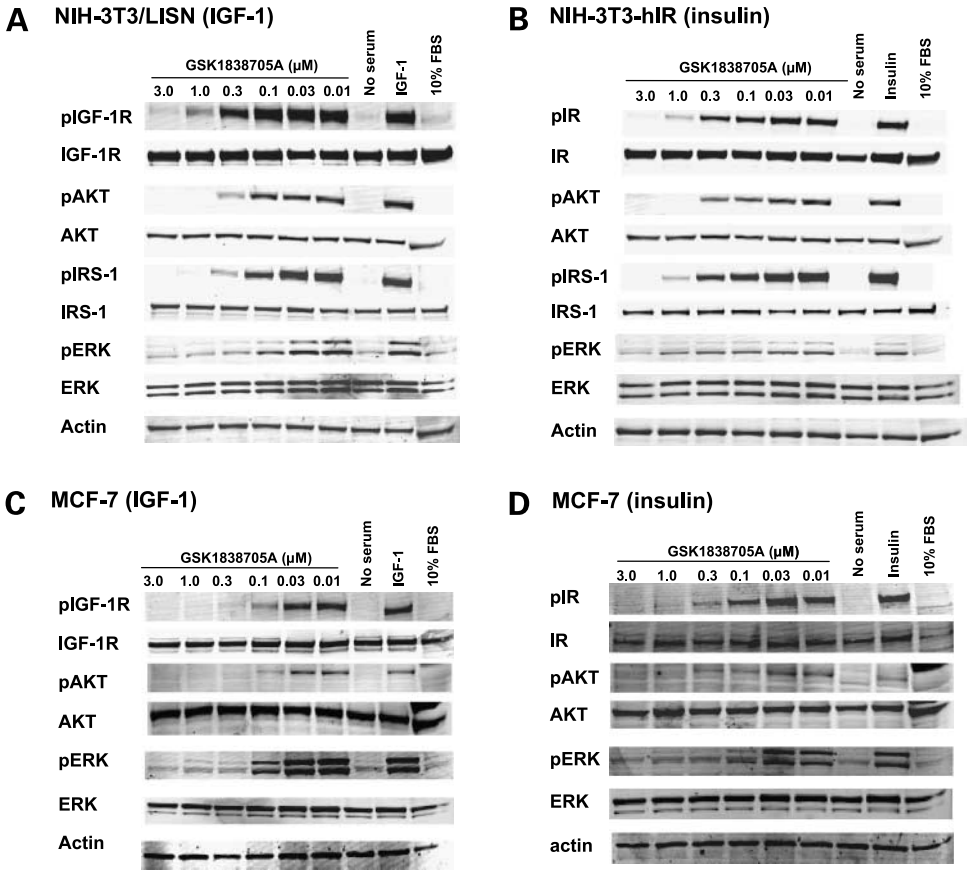

Figure 1. Effect of GSK1838705A on IGF-IR– and IR-mediated signal transduction. NIH-3T3/LISN (**A**), NIH-3T3-hIR (**B**), and MCF-7 (**C** and **D**) cell lines were plated in normal growth medium. After 24 h, the medium was replaced with serum-free medium, and DMSO or GSK1838705A was added to the cells. Four hours later, cells were stimulated with 30 ng/mL IGF-I (**A** and **C**) or 3 μg/mL insulin (**B** and **D**) for 15 min. Whole-cell lysates were resolved by SDS-PAGE and analyzed by Western blotting.

For IR pharmacodynamic studies, a single oral dose of vehicle or GSK1838705A was administered to female nu/nu CD-1 mice. After 4 h, mice were injected with 30 units/kg of human insulin, i.p., and liver tissue was collected after 2 min. Quantification of IR phosphorylation was as described above for IGF-IR, except that the capture plates were prepared for the detection of IR.

GSK1838705A levels were quantified in blood and whole tissue by protein precipitation with acetonitrile followed by high-performance liquid chromatography-tandem mass spectrometry analysis using positive-ion atmospheric pressure chemical ionization or Turbo Ionspray ionization (API 4000 or API5000, Applied Biosystems). The lower limit of quantification of compound was 10 ng/mL, and the assays were linear over a 100- to a 1,000-fold drug concentration range.

Results

Inhibition of Kinase Activity

Small-molecule pyrrolopyrimidines were screened for activity against IGF-IR, which led to the identification of GSK1838705A (Table 1). GSK1838705A is a potent, reversible-binding and ATP-competitive inhibitor with IC_{50}s of 2 ± 0.17 and 1.6 ± 0.18 nmol/L (n = 32) in IGF-IR and IR kinase assays, respectively, as measured by the homogeneous time-resolved fluorescence assay. $^{app}K_i$ values were 0.7 ± 0.2 nmol/L (n = 2) for IGF-IR and 1.1 ± 0.1 nmol/L (n = 3) for IR using the filter binding assay. GSK1838705A was also tested against 45 other serine/threonine and tyrosine kinases and showed weak or no inhibition of these kinases (IC_{50} >1 μmol/L), except ALK, which was inhibited with an IC_{50} of 0.5 nmol/L and a K_i of 0.35 nmol/L (Table 1). Analysis of GSK1838705A in a panel of 224 unique protein kinases (KinaseProfiler, Millipore) showed only 7 additional kinases to be inhibited by >50% at 0.3 μmol/L concentration (Supplementary Table S1). In cellular phosphorylation assays, GSK1838705A potently inhibited IGF-IR and IR phosphorylation with IC_{50}s of 85 ± 38 and 79 ± 43 nmol/L, respectively.

Inhibition of Kinase Signaling

The effect of GSK1838705A on IGF-IR– and IR-mediated signal transduction was assessed in NIH-3T3/LISN and NIH-3T3-hIR cell lines (Fig. 1A and B). Low basal levels of IGF-IR and IR phosphorylation were observed in the absence of serum. On ligand stimulation, a large increase in phosphorylated IGF-IR and IR as well as in AKT, IRS-1, and ERK phosphorylation was observed. GSK1838705A inhibited ligand-induced phosphorylation of IGF-IR and IR in a concentration-dependent manner, with a parallel decrease in phosphorylated AKT, IRS-1, and ERK. Similar results were observed in MCF-7 breast carcinoma cells in response to IGF-I and insulin stimulation (Fig. 1C and D).

Effect on Cell Proliferation

The antiproliferative effect of GSK1838705A was determined in a panel of cell lines derived from solid and hematologic tumors (Table 2). The EC_{50}s of GSK1838705A ranged from ~20 nmol/L to >8 μmol/L, but were <1 μmol/L in most multiple myeloma and Ewing's sarcoma cell lines, consistent with the known dependence of these cell lines on IGF-IR signaling for proliferation (see Discussion). Flow cytometric analysis of MCF-7 and NCI-H929 cells treated with GSK1838705A showed an accumulation of cells predominantly in G_1 (2N) phase of the cell cycle (Supplementary Figs. S1 and S2). In contrast with MCF-7 cells, where there was no increase in cells with sub-2N DNA content with increasing concentration of GSK1838705A, a considerable fraction of cells (20–60%) with sub-2N DNA content, indicative

Table 2. Inhibition of cell growth by GSK1838705A

Tumor	Cell line	EC_{50} (nmol/L)
ALCL	L-82	24 ± 9
	SUP-M2	28 ± 9
	SU-DHL-1	31 ± 7
	KARPAS-299	52 ± 29
	SR-786	88 ± 39
Multiple myeloma	NCI-H929	197 ± 84
	L-363	226 ± 60
	MOLP-8	278 ± 109
	KMS-12-BM	364 ± 84
	EJM	845 ± 202
	LP-1	850 ± 189
	AMO-1	979 ± 357
	JJN-3	2,645 ± 1,296
	HUNS-1	3,971 ± 1,120
Ewing's sarcoma	SK-ES	141 ± 30
	SK-N-MC	155 ± 102
	TC-71	194 ± 55
	RD-ES	207 ± 77
	MHH-ES-1	853 ± 228
	CADO-ES-1	1,008 ± 479
	A673	1,031 ± 482
Colon	HT29	362 ± 241
	COLO 205	644 ± 205
	SW48	773 ± 159
	SW948	875 ± 41
	SW1417	1,716 ± 908
	LS1034	2,794 ± 140
	HCT116	3,311
	SW620	4,736 ± 891
	SW480	7,151 ± 269
	NCI-H747	8,378 ± 2,490
Lung	A549	3,327 ± 1,884
	H1299	5,502 ± 1,005
Breast	MCF-7	203 ± 159
	MX1	209 ± 102
	MDA-MB-468	1,571 ± 690
Cervix	HELA	2,659 ± 1,867
Head and neck	HN5	4,570
Prostate	LNCaP	8,317
Ovary	SKOV	3,052 ± 940
Pancreas	BxPC3	4,224 ± 344
Normal foreskin fibroblast	HFF	1,314 ± 656
Normal prostate epithelium	PREC	1,432 ± 412
Normal umbilical vein endothelium	HUVEC	2,827 ± 905
Normal mammary epithelium	HMEC	3,346 ± 1,367
Mouse fibroblast	NIH-3T3/LISN	1,297 ± 923

NOTE: Data are presented as mean ± SD.

of apoptosis, was detected in NCI-H929 cells treated with 10 μmol/L GSK1838705A (Supplementary Figs. S1 and S2).

Pharmacodynamics and Antitumor Activity *In vivo*

Administration of IGF-I to mice bearing tumor xenografts of NIH-3T3/LISN cells resulted in an ~3-fold induction of IGF-IR phosphorylation (Fig. 2A; Supplementary Fig. S3A). A single oral dose of GSK1838705A at 0.1 and 0.3 mg/kg resulted in 35% and 65% inhibition of IGF-IR phosphorylation, respectively, whereas doses ≥1 mg/kg resulted in complete inhibition of ligand-induced IGF-IR phosphorylation. At a dose of 30 mg/kg, inhibition was sustained for ~24 hours after compound administration (Supplementary Fig. S3A). Analysis of GSK1838705A concentration in blood and tumor 4 hours after administration showed a dose-dependent increase in compound in both tissues beginning at the 3 mg/kg dose, with GSK1838705A concentrations being 3- to 7-fold higher in the tumor tissue than in the blood (Fig. 2A). Blood and tissue levels of the compound were sustained for 8 hours after a single dose of 30 mg/kg (Supplementary Fig. S3A). Inhibition of IGF-IR phosphorylation and downstream signaling (pIRS-1 and pAKT) were also observed in protein immunoblotting studies from GSK1838705A-treated COLO 205 tumor lysates compared with vehicle-treated tumors (Supplementary Fig. S3B). In these studies, clear reduction in phosphorylation was observed at the 30 mg/kg dose, which is higher than the dose required in the NIH-3T3/LISN tumors (Fig. 2A). This may reflect the differences in the cell lines used, differences in the distribution of the compound in the tumors, or differences in the assays used.

Treatment of NIH-3T3/LISN tumor–bearing mice with GSK1838705A at 10, 30, and 60 mg/kg once daily resulted in 17%, 45%, and 77% tumor growth inhibition, respectively, at the end of the treatment period (Fig. 2B). The mice in the 10 and 30 mg/kg treatment groups exhibited very little body weight loss throughout the treatment period. The mice in the 60 mg/kg cohort had a mean body weight loss of 7% after 7 days of treatment, but gradually recovered to the original body weight by the end of the treatment period (Supplementary Fig. S4A). Treatment of COLO 205 tumor–bearing mice with GSK1838705A at 10, 30, and 60 mg/kg once daily resulted in 34%, 80%, and 78% inhibition of tumor growth, respectively, with no effect on body weight (Fig. 2C; Supplementary Fig. S4B). In HT29

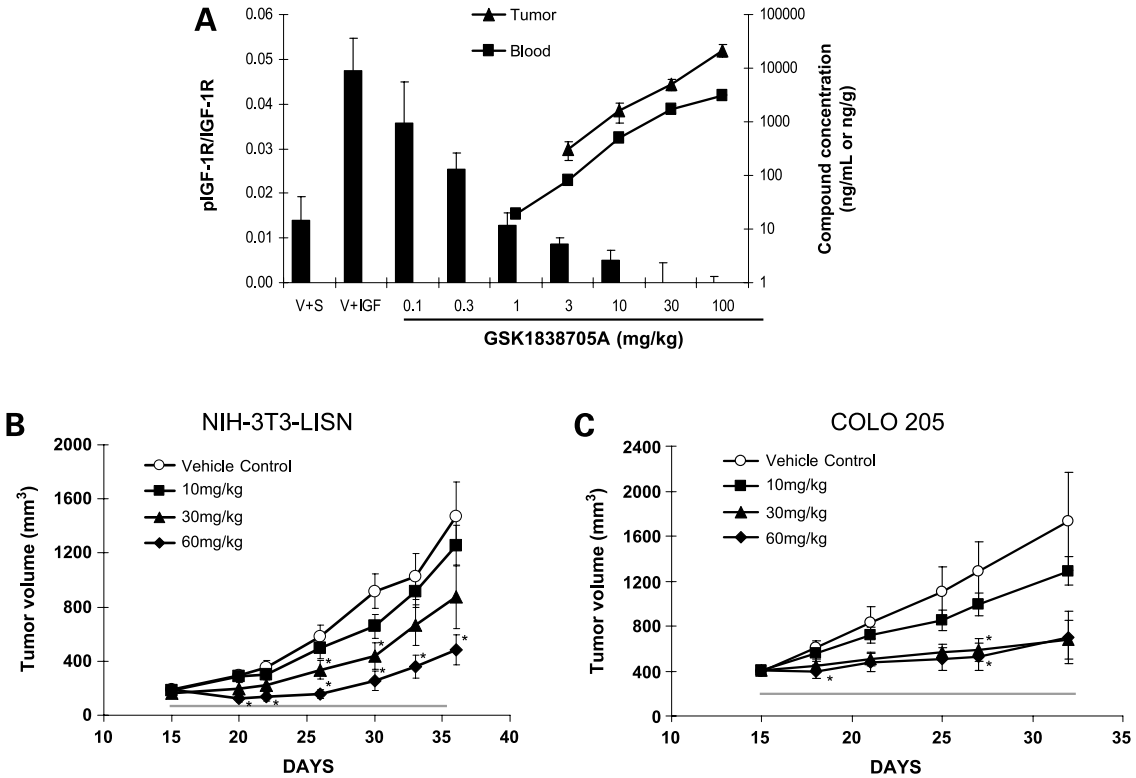

Figure 2. Pharmacodynamics of GSK1838705A and antitumor activity. **A,** effect of GSK1838705A on IGF-IR phosphorylation *in vivo*. Female nude mice bearing NIH-3T3/LISN xenografts (three mice per group) were treated with vehicle (*V*) or GSK1838705A, followed 4 h later by injection of hIGF-I, i.v. Control animals were injected with saline (*V + S*). After 10 min, animals were euthanized, and blood and tumor tissue were collected. Lysates from half of the tumors were analyzed for phospho-IGF-IR and total IGF-IR levels and their ratio is shown (*columns,* mean; *bars,* SD). The amount of compound in the remaining half of the tumor (▲; ng/g) and blood (■; ng/mL) was quantified by high-performance liquid chromatography-tandem mass spectrometry. Missing points indicate that compound concentration was below detection limits. **B** and **C,** *in vivo* efficacy. Female nude mice bearing tumor xenografts of NIH-3T3/LISN (**B**) or COLO 205 (**C**) were treated with vehicle or GSK1838705A (10, 30, or 60 mg/kg), p.o., once daily for 21 d (eight mice per group). Tumors were measured twice per week. *Points,* mean; *bars,* SE. Treatment period is indicated by a gray line at the bottom of the graph. *, $P < 0.05$, Student's *t* test.

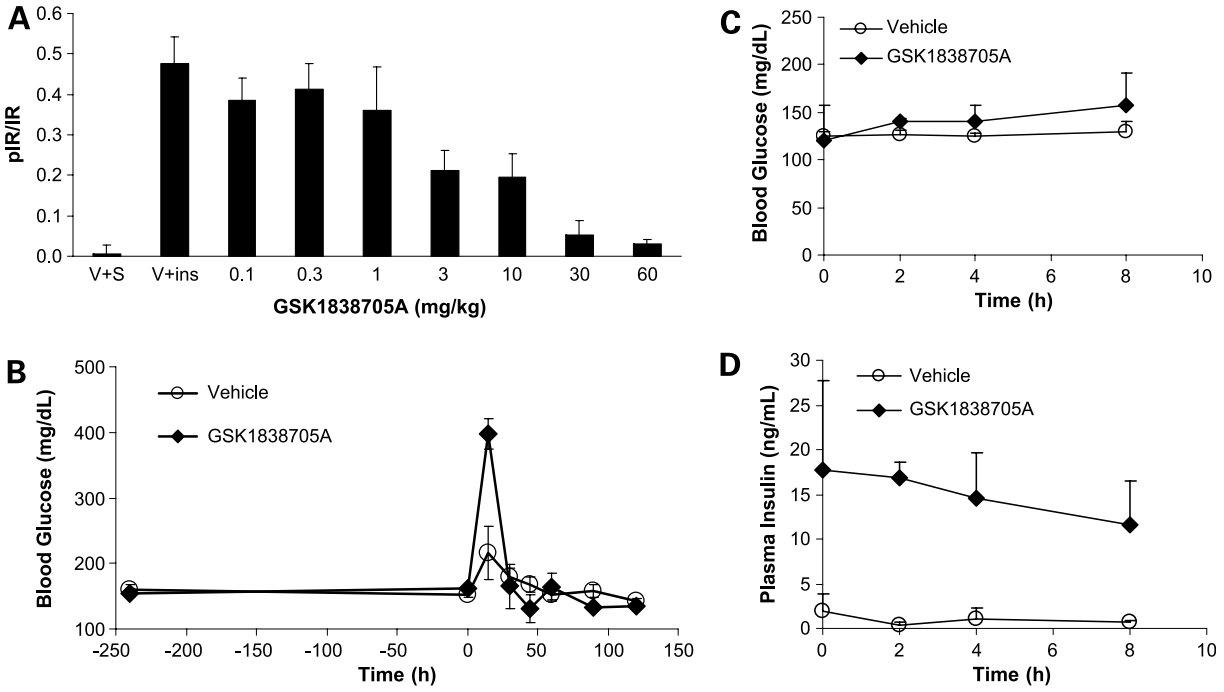

Figure 3. Effect of GSK1838705A on IR phosphorylation and metabolic end points *in vivo*. **A,** effect on IR phosphorylation in liver. Naïve mice (three mice per group) were treated with vehicle (*V*) or GSK1838705A, followed 4 h later with human insulin (*ins*; i.p.). Control animals were injected with saline (*V + S*). Liver tissue was collected after 2 min. *Columns,* mean ratio of phospho-IR to total IR; *bars,* SD). **B,** i.p. glucose tolerance test. Food was withheld for 2 h from female naïve mice (three mice per group) before administering a single dose of vehicle (○) or GSK1838705A (60 mg/kg; ♦). After 4 h, a bolus of glucose (2 g/kg) was given i.p. Blood glucose measurements were taken at various time points. **C** and **D,** effect on blood glucose and insulin levels after chronic treatment. BxPC3 tumor–bearing mice (two mice per group) were treated with vehicle (○) or 60 mg/kg GSK1838705A (♦) once daily. Blood glucose (**C**) and plasma insulin (**D**) measurements were made on day 23 before treatment (time 0; 24 h after the 22nd dose) and at 2 to 8 h after compound administration (food was provided *ad libitum*).

xenograft–bearing mice, 60 mg/kg GSK1838705A caused a 42% tumor growth inhibition relative to vehicle-treated controls at the end of the treatment period, with no significant changes in body weight (Supplementary Fig. S5A and B). In animals bearing BxPC3 xenografts, tumor growth inhibition at the end of the treatment period was 56% and 60% with doses of 30 and 60 mg/kg, respectively. A 5% decrease in animal weight was observed initially at the 60 mg/kg dose, with no further decrease with continued treatment (Supplementary Fig. S5C and D). The antitumor efficacy of GSK1838705A is consistent with the concentration of GSK1838705A in blood and tumors (Fig. 2A). At all doses above 30 mg/kg, blood and tumor concentrations of the compound were higher than the IC_{50} for the cell lines in cell proliferation assays (Table 2). Furthermore, at the 30 mg/kg dose, these levels were sustained for 8 to 24 hours, supporting once-daily administration.

Effect of IGF-1R/IR Inhibition on Blood Glucose Levels

Glucose homeostasis is maintained through the insulin-mediated uptake of glucose in skeletal muscle and the suppression of glucose production in the liver (17). Therefore, both skeletal muscle and liver are appropriate target organs in which to assess the effects of GSK1838705A on IR inhibition *in vivo*. Administration of bolus insulin resulted in an increased phosphorylation of IR, which was inhibited by pretreatment of mice with GSK1838705A in a dose-dependent manner in liver (Fig. 3A) and muscle (data not shown).

To characterize the effect of GSK1838705A on glucose homeostasis, an i.p. glucose tolerance test was done (Fig. 3B). Mice pretreated with 60 mg/kg of GSK1838705A showed a 2-fold increase in peak blood glucose levels (15 minutes following glucose administration) when compared with vehicle-treated mice. However, this returned to baseline within 30 minutes, similar to vehicle-treated animals, suggesting a minimal effect on glucose homeostasis at a biologically effective dose.

To address the metabolic effects of chronic treatment with GSK1838705A, blood glucose and insulin levels were measured after 23 days of treatment with GSK1838705A (Fig. 3C and D). Blood glucose levels were not elevated in GSK1838705A-treated animals at time 0 (24 hours after the 22nd dose), relative to vehicle-treated animals, and showed no significant change over the following 8 hours. However, insulin levels were substantially higher at time 0 and remained elevated at 8 hours. When GSK1838705A was administered continuously for 8 days, there was no increase in insulin levels at time 0 (24 hours after the 7th dose), although transient increases in glucose and insulin levels were observed with a peak at 2 hours after the 8th dose (Supplementary Fig. S6A and B). Furthermore, there was no change in β-hydroxybutyrate levels, used to monitor ketosis that occurs as a result of a blockade of glucose uptake by the cell (Supplementary Fig. S6C). These data

indicate that GSK1838705A has a transient and modest effect on blood glucose levels, probably due to its effects on IR signaling, and that the chronic administration leads to hyperinsulinemia to maintain glucose homeostasis.

Effect on Tumor Cells with Activated ALK

Because GSK1838705 showed potent inhibition of ALK activity, we evaluated its effect on tumor cell lines harboring ALK fusion genes, which results in activated ALK. Proliferation of ALCL cell lines expressing the nucleophosmin (NPM)-ALK fusion (18, 19) was inhibited by GSK1838705A in a concentration-dependent manner (EC_{50}s 24–88 nmol/L; Supplementary Fig. S7A; Table 2), whereas FE-PD ALCL cells lacking the fusion (18) were relatively insensitive, with an EC_{50} of 4.4 μmol/L (Supplementary Fig. S7A). H2228 NSCLC cells, expressing the echinoderm microtubule-associated protein-like 4 (EML4)-ALK fusion gene (20), were also sensitive to GSK1838705A in the proliferation assay (IC_{50}, 191 ± 34 nmol/L; n = 2). Treatment of cells with IGF-IR inhibitors lacking ALK activity had no effect on proliferation (data not shown), confirming the role of ALK in driving the proliferation of these cells. In flow cytometry analyses, treatment of the ALCL cell line Karpas-299 with GSK1838705A resulted in increase in cells with 2N and <2N DNA content, indicative of cell cycle arrest and apoptosis (Supplementary Fig. S7B).

The effect of GSK1838705A on ALK phosphorylation in cells was determined in Karpas-299 and SR-786 ALCL cell lines. Phosphorylation of NPM-ALK and the downstream transcription factor signal transducer and activator of transcription 3 (STAT3) was decreased in a concentration-dependent manner in both cell lines by GSK1838705A (Supplementary Fig. S8A and B). In quantitative assays, GSK1838705A inhibited NPM-ALK phosphorylation in Karpas-299 and SR-786 cells with an IC_{50} of 20.5 ± 13.2 nmol/L (n = 4) and 31 nmol/L (n = 1), respectively, which is consistent with the ability of GSK1838705A to inhibit proliferation of ALCL cell lines (Table 2). It also inhibited phosphorylation of EML4-ALK in H2228 cells with an IC_{50} of 31 nmol/L (n = 2); however, there was only a modest effect on STAT3 phosphorylation in this cell line (Supplementary Fig. S8C).

To further characterize the effect of GSK1838705A on ALK-driven tumors, tumor xenograft studies were conducted in mice bearing Karpas-299 and SR-786 tumors. GSK1838705A showed a dose-dependent effect on the

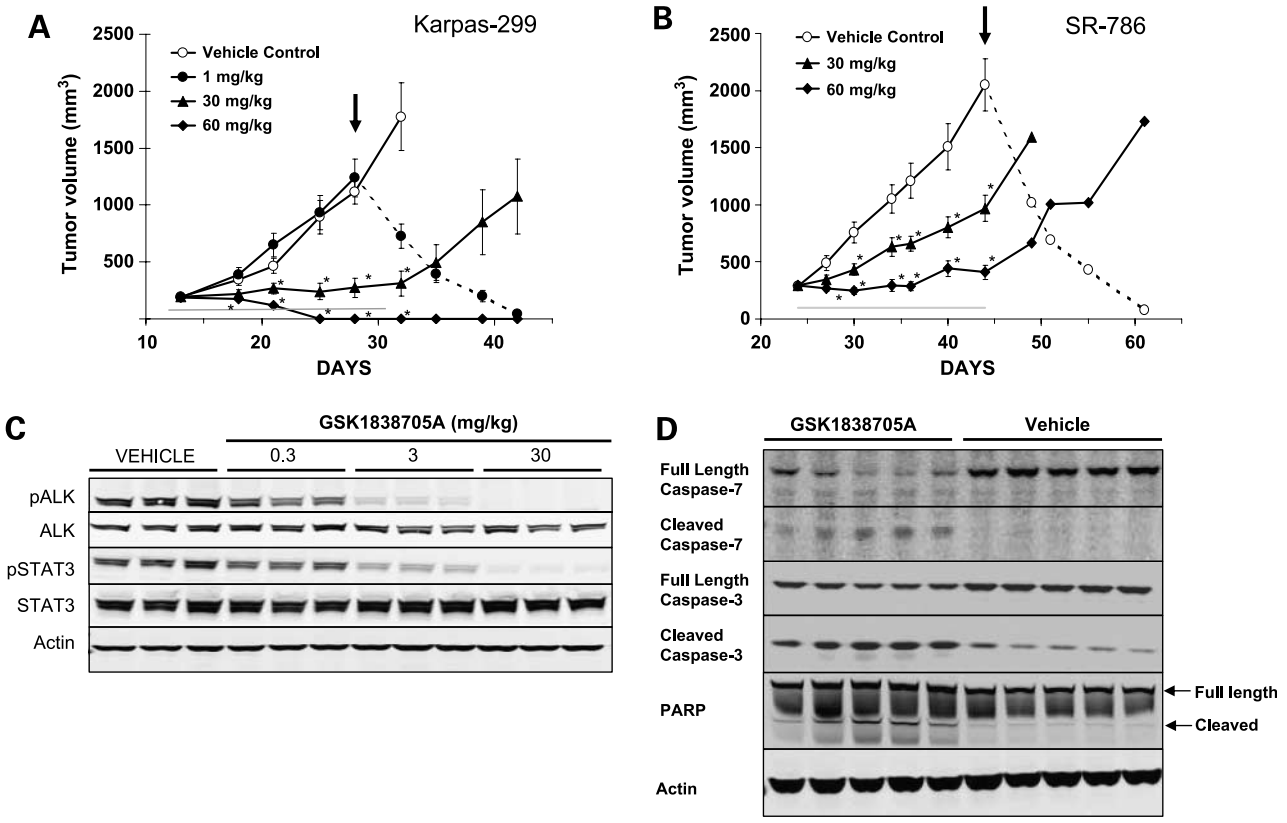

Figure 4. Antitumor efficacy of GSK1838705A in ALK-dependent tumor xenografts. Female SCID mice bearing Karpas-299 (**A**) or SR-786 (**B**) tumor xenografts were treated with vehicle or GSK1838705A, p.o., once daily for 21 d. *Points,* mean from eight mice per group; *bars,* SE. *Arrow,* the point at which the dose was switched from the 1 mg/kg to the 60 mg/kg once daily regimen (for Karpas-299), or from vehicle to the 100 mg/kg once daily regimen (for SR-786). *Dotted line,* subsequent tumor measurements. *, $P < 0.05$, Student's t test. **C,** inhibition of signal transduction. Mice bearing Karpas-299 tumor xenografts were treated with vehicle or a single dose of GSK1838705A (three mice per group). Tumor lysates were prepared after 4 h and analyzed by Western blotting. **D,** induction of apoptosis. Mice bearing Karpas-299 tumor xenografts were treated with vehicle or 60 mg/kg GSK1838705A for 5 d (five mice per group). Tumor lysates were prepared 4 h after the final dose and analyzed by Western blotting. Each lane represents a sample from a different mouse in that group.

growth of established Karpas-299 xenografts with 22% and 93% tumor growth inhibition at 10 and 30 mg/kg once-daily administration of GSK1838705A, respectively (Fig. 4A and data not shown). Tumor growth resumed after discontinuation of the 30 mg/kg dose, suggesting that sustained treatment is required at this dose. A dose of 60 mg/kg, however, resulted in complete regression of tumor growth, and all animals remained tumor-free 9 days after treatment was discontinued. Based on these results, on day 16 of treatment, the 1 mg/kg cohort was switched to a 60 mg/kg dose, which resulted in a gradual decrease in tumor volume over the next 14 days, with complete tumor regression observed in seven of the eight mice (Fig. 4A). In animals bearing SR-786 xenografts, tumor growth inhibition of 63% and 93% was observed with 30 and 60 mg/kg once-daily administration of GSK1838705A, respectively (Fig. 4B). Substantial tumor regression was observed when animals in the vehicle control group bearing large tumors (~2,000 mm^3) were subsequently treated with 100 mg/kg GSK1838705A once daily. Three of eight animals in this group showed complete regression of their tumors by day 61 (Fig. 4B). GSK1838705A treatment had no effect on weights of the animals in these studies (Supplementary Fig. S4C and D).

Inhibition of tumor growth was associated with a decrease in ALK signaling in Karpas-299 tumor xenografts (Fig. 4C). Substantial reduction in phosphorylated ALK and STAT3 was observed at doses ≥3 mg/kg. Furthermore, cleavage products of caspase-3, caspase-7, and poly(ADP-ribose) polymerase were detected in tumors treated with GSK1838705A, providing evidence for induction of apoptosis in ALK-dependent tumors (Fig. 4D).

Discussion

GSK1838705A potently inhibits IGF-IR, IR, and ALK signaling in cells; inhibits the proliferation of cancer cell lines; and compromises the growth of tumor xenografts in nude mice. A structurally distinct IGF-IR–selective inhibitor previously described, GSK1904529A, showed similar potent activity against IGF-IR and IR, but lacked activity against ALK (21, 22). Both compounds inhibited IGF-IR signaling in cells, although GSK1904529A seemed to be more potent than GSK1838705A. Consistent with this, GSK1904529A also seemed to be more potent than GSK1838705A in the cell proliferation assays. This may be due to differences in cell permeation. However, the observation that a common group of cell lines (with the exception of the ALK-dependent tumors) is sensitive to the two structurally distinct inhibitors with different kinase-selectivity profiles suggests that inhibition of IGF-IR plays a causal role in cell growth inhibition in these cell lines. In addition, the observation that GSK1904529A does not inhibit the growth of the ALCL cell lines confirms the role of ALK in driving the proliferation of these cells.

Despite the fact that GSK1838705A inhibited IGF-IR and IR kinase activities with similar potencies and reduced IR activity *in vivo*, it did not cause sustained increase in blood glucose levels. It was anticipated that an ATP-competitive IGF-IR inhibitor, such as GSK1838705A, would inhibit both IGF-IR and IR kinase activities with similar potencies, as these receptors share 85% sequence homology in the kinase domains and have identical ATP binding clefts (23). Therefore, the lack of a hyperglycemic response by GSK1838705A is unexpected. The transient increase in blood glucose, especially in the glucose tolerance test, clearly suggests the perturbation of insulin signaling. Similar results were observed with the structurally distinct IGF-IR/IR inhibitors GSK1904529A (22) and NVP-AEW541 (24). The increase in insulin levels provides a potential explanation for the minimal change in blood glucose; however, the sustained hyperinsulinemia in mice treated for 23 days, compared with 8 days, suggests that caution is warranted with chronic dosing. Alternate treatment regimens should be considered to minimize long-term metabolic alteration while optimizing the antitumor effect. Concomitant treatment with antidiabetic agents should also be evaluated to further explore ways to minimize metabolic liabilities of agents targeting IGF-IR and IR.

In addition to its role in glucose metabolism, recent evidence implicates a role for IR signaling in cancer (25). IR-A, an isoform of IR, binds to IGF-II and serves as a second physiologic receptor for this ligand. Furthermore, IR-A heterodimerizes with IGF-IR, and these hybrid receptors can stimulate cell motility in response to IGF-II, IGF-I, and insulin (26, 27). Thus, the antitumor activity of ATP-competitive IGF-IR inhibitors such as GSK1838705A may be mediated, in part, through inhibition of IR or IR/IGF-IR heterodimers. Moreover, this ability to inhibit both IGF-IR and IR kinase activities represents a potential therapeutic advantage over anti–IGF-IR monoclonal antibodies.

Ewing's sarcoma and multiple myeloma have been shown to be sensitive to growth inhibition by IGF-IR–targeted therapeutic agents (28–32). Consistent with these findings, we found that several cell lines derived from multiple myeloma and Ewing's sarcoma were sensitive to GSK1838705A. IGF-IR has been shown to play an important role in the growth and survival of human multiple myeloma cell lines (31, 32). Moreover, recent clinical data indicate that treatment of multiple myeloma patients with IGF-IR monoclonal antibodies in combination with dexamethasone leads to partial and complete responses (33). In spite of the general sensitivity of multiple myeloma cell lines to GSK1838705A, the HUNS-1 and JJN-3 lines were relatively resistant to GSK1838705A-induced growth inhibition (EC_{50}s of 3,971 and 2,645 nmol/L, respectively). The CD45 protein tyrosine phosphatase negatively regulates IGF-IR signaling in multiple myeloma cells, and IGF-IR antibodies do not inhibit the growth of $CD45^+$ multiple myeloma cells (34, 35). The HUNS-1 cell line has high CD45 protein levels compared with the more sensitive NCI-H929, LP-1, and L363 multiple myeloma cell lines, and this may explain the lack of sensitivity of HUNS-1 cells to GSK1838705A (data not shown). However, further studies will be required to substantiate this possibility.

The IGF-IR signaling pathway is also involved in the growth, invasion, and metastasis of Ewing's sarcoma (36). Translocation between the *EWS* gene and the FLI1

transcription factor is observed in a large majority of Ewing's family tumors, and this fusion gene is required for the survival of Ewing's sarcoma cells (37–39). EWS-FLI1 has been shown to transcriptionally repress IGFBP-3, the main circulating carrier protein for IGFs (39). Thus, transcriptional repression of IGFBP-3 by EWS-FLI1 could reactivate the IGF-IR signaling pathway and confer dependency on IGF-IR for cell growth. Although all the Ewing's sarcoma cell lines used in our study harbored *EWS-FLI1* fusion gene, they were not equally sensitive to growth inhibition by GSK1838705A, suggesting potential contribution from other signaling pathways besides IGF-IR in these cell lines. EWS-FLI1 has been shown to transactivate the expression of a number of genes beyond those regulated by IGF-IR, which could contribute to the aberrant growth of Ewing's sarcoma cells (40).

ALK is a receptor tyrosine kinase in the IR family, which is aberrantly activated by gene fusion in ALCL and in a subset of NSCLC (41–43). Fusion of ALK with NPM and EML4 has been observed in ALCL and NSCLC, respectively, and fusions with other genes have also been identified in patients with these and other malignancies (44). More recently, both germ-line and somatic mutations in *ALK* gene have been reported in neuroblastoma patients (45). IGF-IR and IR share a high degree of sequence homology with ALK kinase, and thus, it was not surprising that GSK1838705 also inhibits ALK kinase, although other small-molecule IGF-IR inhibitors have not reported activity against ALK. The exceptional potency of GSK1838705A in ALCL and NSCLC cell lines containing ALK fusion genes and the complete regression of NPM-ALK–dependent tumors in mice with GSK1838705A are encouraging findings for the treatment of cancers driven by oncogenic ALK. These data are consistent with the antiproliferative effects of other ALK kinase inhibitors observed in tumor cell lines harboring ALK fusion genes (18, 42, 46).

In summary, we have shown that GSK1838705A is a potent and selective modulator of IGF-IR activity, with robust antitumor activity in animal xenograft models. Tumor types likely to respond to GSK1838705A include multiple myeloma and Ewing's sarcoma, as well as ALK-driven tumors (e.g., ALCL, NSCLC, and neuroblastoma). Efforts are ongoing to identify additional sensitive tumor types, as well as a molecular signature for sensitivity and resistance to GSK1838705. Combination therapy using GSK1838705A with cytotoxic agents and other signaling inhibitors should also be evaluated.

Disclosure of Potential Conflicts of Interest

All authors are current or former employees of GlaxoSmithKline.

References

1. Pollak MN, Schernhammer ES, Hankinson SE. Insulin-like growth factors and neoplasia. Nat Rev Cancer 2004;4:505–18.

2. Hartog H, Wesseling J, Marike BH, van der Graaf WTA. The insulin-like growth factor 1 receptor in cancer: old focus, new future. Eur J Cancer 2007;43:1895–904.

3. Renehan AG, Zwahlen M, Minder C, O'Dwyer ST, Shalet SM, Egger M. Insulin-like growth factor-1, IGF binding protein 3, and cancer risk: systematic review and meta-regression analysis. Lancet 2004;363:1346–53.

4. Weber MM, Fottner C, Liu SB, Jung MC, Engelhardt D, Baretton GB. Overexpression of the insulin-like growth factor 1 receptor in human colon carcinomas. Cancer 2002;95:2086–95.

5. Valentini B, Baserga R. IGF-I receptor signalling in transformation and differentiation. J Clin Pathol 2001;54:133–7.

6. Hoffmann F, Garcia-Echeverria C. Blocking insulin-like growth factor-1 receptor as a strategy for targeting cancer. Drug Discov Today 2005;10:1041–7.

7. Baserga R, Peruzzi F, Reiss K. The IGF-1 receptor in cancer biology. Int J Cancer 2003;107:873–7.

8. Resnicoff M, Coppola D, Sell C, Rubin R, Ferrone S, Baserga R. Growth inhibition of human melanoma cells in nude mice by antisense strategies to the type 1 insulin-like growth factor receptor. Cancer Res 1994;54:4848–50.

9. Sachdev D. Drug evaluation: CP-751871, a human antibody against type I insulin-like growth factor receptor for the potential treatment of cancer. Curr Opin Mol Ther 2007;9:299–304.

10. Olmos D, Okuno S, Schuetze SM, et al. Safety, pharmacokinetics and preliminary activity of the anti-IGF-1R antibody CP-751,871 in patients with sarcoma. J Clin Oncol 2008;26:10501.

11. Karp DD, Paz-Ares LG, Novello S, et al. High activity of the anti-IGF-1R antibody CP-751,871 in combination with paclitaxel and carboplatin in squamous NSCLC. J Clin Oncol 2008;26:8015.

12. Jones HE, Goddard L, Gee JM, et al. Insulin-like growth factor-1 receptor signalling and acquired resistance to gefitinib (ZD1839; Iressa) in human breast and prostate cancer cells. Endocr Relat Cancer 2004;11:793–814.

13. Nahta R, Yu D, Hung M-C, Hortobyagi GN, Esteva FJ. Mechanisms of disease: understanding resistance to HER2-targeted therapy in human breast cancer. Nature Clin Prac 2006;3:269–80.

14. Milano A, Dal Lago L, Sotiriou C, Piccart M, Cardoso F. What clinicians need to know about antiestrogen resistance in breast cancer. Eur J Cancer 2006;42:2692–705.

15. Kaleko M, Rutter W, Miller D. Overexpression of the human insulinlike growth factor I receptor promotes ligand-dependent neoplastic transformation. Mol Cell Biol 1990;10:464–73.

16. Vindelov LI, Christensen IJ, Jensen J, Nissen NI. Limits of detection of nuclear DNA abnormalities by flow cytometric DNA analysis: results obtained by a set of methods for sample-storage, staining and international standardization. Cytometry 1983;3:332–8.

17. Kim J, Wei Y, Sowers JR. Role of mitochondrial dysfunction in insulin resistance. Circ Res 2008;102:401–14.

18. Galkin AV, Melnick JS, Kim S, et al. Identification of NVP-TAE684, a potent, selective, and efficacious inhibitor of NPM-ALK. Proc Natl Acad Sci U S A 2007;104:270–5.

19. Dirks WG, Fahnrich S, Lis Y, Becker E, Macleod AF, Drexler HG. Expression and functional analysis of the anaplastic lymphoma kinase (ALK) gene in tumor cell lines. Int J Cancer 2002;100:49–56.

20. Koivunen JP, Mermel C, Zejnullahu K, et al. *EML4-ALK* fusion gene and efficacy of an ALK kinase inhibitor in lung cancer. Clin Cancer Res 2008;14:4275–83.

21. Chamberlain S, Wilson JW, Deanda F, et al. Discovery of 4,6-bis-anilino-1*H*-pyrrolo(2,3-*d*] pyrimidines: potent inhibitors of the IGF-1R receptor tyrosine kinase. Bioorg Med Chem Lett 2008;19:469–73.

22. Sabbatini P, Rowand JL, Groy A, et al. Antitumor activity of GSK1904529A, a small-molecule inhibitor of the insulin-like growth factor-I receptor tyrosine kinase. Clin Cancer Res 2009;15:3058–67.

23. Ullrich A, Gray A, Tam AW, et al. Insulin-like growth factor 1 receptor primary structure: comparison with insulin receptor suggests structural determinants that define functional specificity. EMBO J 1986;5:2503–12.

24. Garcia-Echeverria C, Pearson MA, Marti A, et al. *In vivo* antitumor activity of NVP-AEW541-A novel, potent, and selective inhibitor of the IGF-1R kinase. Cancer Cell 2004;5:231–9.

25. Belfiore A. The role of insulin receptor isoforms and hybrid insulin/IGF-1 receptors in human cancers. Curr Pharm Des 2007;13:671–86.

26. Pandini G, Vigneri R, Costantini A, et al. Insulin and insulin-like growth factor-1 (IGF-1) receptor overexpression in breast cancer leads to insulin/IGF-1 hybrid receptor overexpression: evidence for a second mechanism of IGF-1 signaling. Clin Cancer Res 1999;5:1935–44.

27. Pandini G, Frasca F, Mineo R, Sciacca L, Vigneri R, Belfiore A. Insulin and insulin-like growth factor 1 hybrid receptors have different biological characteristics depending on the insulin receptor isoform involved. J Biol Chem 2002;277:39684–95.

28. Benini S, Manara MC, Baldini N, et al. Inhibition of insulin-like growth factor 1 receptor increases the antitumor activity of doxorubicin and vincristine against Ewing's sarcoma cells. Clin Cancer Res 2001;7:1790–7.

29. Manara MC, Landuzzi L, Nanni P, et al. Preclinical *in vivo* study of new insulin-like growth factor 1 receptor-specific inhibitor in Ewing's sarcoma. Clin Cancer Res 2007;13:11322–30.

30. Scotlandi K, Manara MC, Nicoletti G, et al. Antitumor activity of the insulin-like growth factor 1 receptor kinase inhibitor NVP-AEW541 in musculoskeletal tumors. Cancer Res 2005;65:3868–76.

31. Mitsiades CS, Mitsiades NS, McMullan CJ, et al. Inhibition of the insulin-like growth factor receptor-1 tyrosine kinase activity as a therapeutic strategy for multiple myeloma, other hematological malignancies, and solid tumors. Cancer Cell 2004;5:221–30.

32. Georgii-Hemming P, Wiklund HJ, Ljunggren O, Nilsson K. Insulin-like growth factor 1 is a growth and survival factor in human multiple myeloma cell lines. Blood 1996;88:2250–8.

33. Lacy MQ, Alsina M, Fonseca R, et al. Phase I, pharmacokinetic and pharmacodynamic study of the anti-insulinlike growth factor type 1 receptor monoclonal antibody CP-751,871 in patients with multiple myeloma. J Clin Oncol 2008;26:3196–203.

34. Deschamps G, Pellat-Deceunynck C, Szpak Y, Bataille R, Robillard N, Amiot M. The magnitude of Akt/phosphatidylinositol 3′ kinase proliferating signalling is related to CD45 expression in human myeloma cells. J Immunol 2004;173:4953–9.

35. Deschamps G, Wuilleme-Toumi S, Trichet V, et al. CD45neg but not CD45pos human myeloma cells are sensitive to the inhibition of IGF-1 signaling by a murine anti-IGF-1R monoclonal antibody, mAVE1642. J Immunol 2006;177:4953–9.

36. Leavey PJ, Collier AB. Ewing sarcoma: prognostic criteria, outcomes and future treatment. Expert Rev Anticancer Ther 2008;8:617–24.

37. Arvand A, Denny CT. Biology of EWS/ETS fusions in Ewing's family tumors. Oncogene 2001;20:5747–54.

38. Yi H-K, Fujimura Y, Ouchida M, Prasad DDK, Rao VN, Reddy ESP. Inhibition of apoptosis by normal and aberrant Fli-1 and erg proteins involved in human solid tumors and leukemias. Oncogene 1997;14:1259–68.

39. Prieur A, Tirode F, Cohen P, Delattre O. EWS/FLI-1 silencing and gene profiling of Ewing cells reveal downstream oncogenic pathways and a crucial role for repression of insulin-like growth factor binding protein 3. Mol Cell Biol 2004;24:7275–83.

40. Smith R, Owen LA, Trem DJ, et al. Expression profiling of EWS/FLI identifies NKX2.2 as a critical target gene in Ewing's sarcoma. Cancer Cell 2006;9:405–16.

41. Soda M, Choi YL, Enomoto M, et al. Identification of the transforming EML4-ALK fusion gene in non-small-cell lung cancer. Nature 2007;448:561–6.

42. Li R, Morris SW. Development of anaplastic lymphoma kinase (ALK) small-molecule inhibitors for cancer therapy. Med Res Rev 2008;28:372–412.

43. Amin HM, Lai R. Pathobiology of ALK^+ anaplastic large-cell lymphoma. Blood 2008;110:2259–67.

44. Chiarle R, Voena C, Ambrogio C, Piva R, Inghirami G. The anaplastic lymphoma kinase in the pathogenesis of cancer. Nat Rev Cancer 2008;8:11–23.

45. Mosse Y, Laudenslager M, Longo L, et al. Identification of ALK as a major familial neuroblastoma predisposition gene. Nature 2008;455:930–5.

46. Christenson JG, Zou HY, Arango ME, et al. Cytoreductive antitumor activity of PF-2341066, a novel inhibitor of anaplastic lymphoma kinase and c-met, in experimental models of anaplastic large-cell lymphoma. Mol Cancer Ther 2007;6:3314–22.